Chapter 2
Processes and Procedures

2.1 AVO processing

The surface seismic data processed through full pre-stack time migration with relative amplitude preservation still contained significant amount of multiples. Therefore, a parabolic Radon demultiple technique had been applied to remove them. The generalized Radon transforms, commonly known as τ-p transforms, are often used in seismic data processing for multiple suppression and signal enhancement. The general theory of Radon transforms can be found in Deans (1983). Durrani and Bisset (1984) examined the fundamental properties of various Radon transforms. In seismic applications, there are mainly three τ-p transforms: linear, parabolic and hyperbolic. The parabolic Radon transform is defined as

$$R_{p\tau}\{f(x,t)\} = \int_{-\infty}^{\infty} f(x, \tau + px^2)dx, \qquad (2.1)$$

where $f(x,t)$ portrays a 2-D function in R^2 domain $(\forall x, t)$ and where the t coordinate of $f(x,t)$ occurs on the line $t = \tau + px^2$ in $x - t$ space.

In this study, two 2-D surface seismic lines (Figure 2.1) were extracted from pre-stack time migrated cube and additionally processed through velocity analysis, normal moveout (NMO) correction, mute, parabolic Radon-transform demultiple, and stack.

2.1.1 Velocity analysis

The velocity analysis was done at every 20 CDP location for line A (500-m interval) and at every 40 CDP location for line B (500-m interval). The main criterion for picking of time-velocity functions at each location was flattening of primary events.

2.1.2 NMO correction

The NMO corrections for both lines were carried out using the picked time-velocity functions of each line. Velocities at in-between points were interpolated and outside extrapolated.

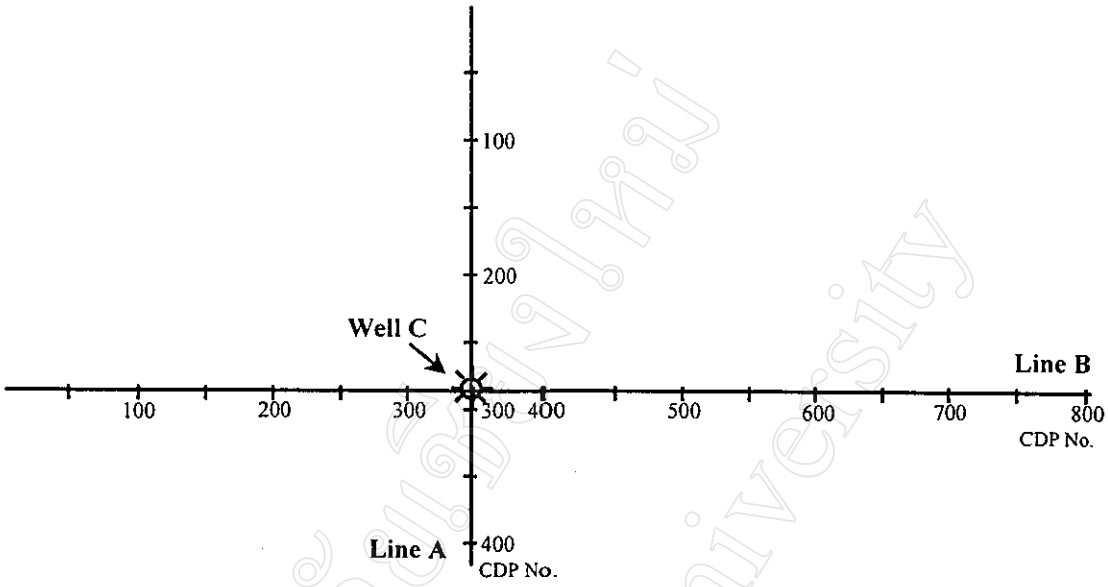

Figure 2.1 The schematic map of Line A and B including Well C location and CDP numbers.

2.1.3 Mute

An optimum mute pattern was picked and applied after NMO corrections to remove noises and excessive NMO stretches. The outside mute trend is within the 45-degree far-angle band.

2.1.4 Parabolic Radon-transform demultiple

A parabolic Radon-transform demultiple process was applied to remove multiple reflections remaining in the processed data. The selected parameters for the program are shown in Table 2.1.

2.1.5 Stack

Stacking is the process of summing all traces in each CDP gather. So it produces a single trace at a single CDP location. It improves signal to noise ratio and suppresses multiples rather significantly.

2.2 AVO angle stacks

The final CDP gathers after Radon-transform demultiple were assigned with three mute patterns for propagation angle bands; 0-15° (near angle), 15°-30° (middle angle), and 30°-45° (far angle). These propagation angle bands are equal to incidence angle

bands of 0-7.6°, 7.6°-16.1°, and 16.1°-26.6° respectively. The checkshot velocity function from Well C was used to convert time to depth in order to compute the angle-band mute patterns. Then inside and outside mutes were applied to CDP gathers for each angle-band stacking. Table 2.2 shows the time-offset values of the three propagation angle bands.

2.3 AVO modeling

For AVO modeling and analysis in the area, sets of dipole shear wave log (DSI) were acquired in addition to routine suite of logs at Well C. Zoeppritz equations AVO modeling and full elastodynamic modeling were performed using the picked in-situ values of P-wave velocity, S-wave velocity, and density. A single set of values was picked at the most representative portion of each sand or shale formation.

2.3.1 Full Zoeppritz AVO modeling

Zoeppritz-equations AVO modeling was performed for selected sand and coal beds to evaluate individual unit's theoretical AVO response. The exact Zoeppritz equations were used for a single-boundary half-space model with the picked log values (Table 2.3).

Using the Zoeppritz equations, the reflection coefficients were computed for incident angles from 0 to 30° in order to correlate with the surface seismic data that have an outside mute equivalent to about 27°. The computed reflection coefficients were plotted out to show the theoretical AVO trends of all picked sand and coal formations.

Apart from the full Zoeppritz equations, other approximated equations such as Aki and Richards (1980), Sheuy (1985), and Hilterman (1983) were also applied for gas sand 2, wet sand 2, and coal 2. The computation were done up to incident angle 60°.

The Aki and Richard's approximation is

$$R_{PP}(\theta) \approx \frac{1}{2}(1 - 4p^2 V_{Sa}^2)\left(\frac{\Delta\rho}{\rho_a}\right) + \frac{1}{2\cos^2\theta}\left(\frac{\Delta V_P}{V_{pa}}\right) - 4\rho^2 V_{Sa}^2 \frac{\Delta V_s}{V_{Sa}}, \quad (2.2)$$

the Shuey's approximation is

Table 2.1 Selected parameters for the parabolic Radon-transform demultiple.

Parameters	Optimal Values
• Reference maximum offset to which maximum and minimum moveout times are associated	3200 m
• Intercept offset to which $\tau - p$ times are associated	0 m
• Minimum moveout time on reference offset	-50 ms
• Maximum moveout time on reference offset	600 ms
• Moveout time increment on reference offset	16 ms
• Moveout time on reference offset where multiples begin at maximum time, 5 sec	80 ms
• Moveout time on reference offset where multiples begin at zero time, 0 sec	200 ms

Table 2.2 Time-offset values for the three angle-band mute patterns.

Two-way time (sec)	Depth (m)	Offset (m)			
		0°	15°	30°	45°
0.0	0	0	0	0	0
0.5	429	0	115	248	429
0.9	843	0	226	487	843
1.1	1090	0	292	629	1090
1.3	1366	0	366	789	1366
1.5	1673	0	448	966	1673
1.7	2006	0	538	1158	2006
1.9	2363	0	633	1364	2363
2.5	3500	0	938	2021	3500
3.0	4311	0	115	2489	4311
4.0	6381	0	1710	3684	6381
5.0	9444	0	2531	5457	9444

Table 2.3 Velocity and density parameters of gas sands, wet sands, and coal beds used in the Zoeppritz-equations AVO modeling. The most representative values were picked from the logs at Well C.

Unit layer	V_p (m/s)	V_s (m/s)	Density (g/cm^3)
Shale	3116.0	1689.0	2.460
Gas Sand 1	3214.3	1919.7	2.184
Shale	3429.4	1735.6	2.620
Gas Sand 2	3308.7	2046.9	2.230
Shale	3508.3	1706.6	2.575
Gas Sand 3	3305.5	2039.5	2.212
Shale	2690.9	1334.6	2.380
Wet Sand 1	2547.4	1386.9	2.052
Shale	3187.8	1614.2	2.451
Wet Sand 2	2748.8	1540.4	2.070
Shale	3320.9	1901.5	2.338
Wet Sand 3	3201.1	1879.1	2.207
Shale	3477.0	1736.6	2.605
Wet Sand 4	3218.4	1884.4	2.215
Shale	3197.4	1698.5	2.393
Coal Bed 1	2544.4	1279.1	1.788
Shale	3132.3	1616.3	2.480
Coal Bed 2	2577.4	1264.1	1.621
Shale	3165.3	1638.5	2.500
Coal Bed 3	2542.6	1297.1	1.664
Shale	3045.5	1642.9	2.396
Coal Bed 4	2689.1	1358.7	1.691
Shale	3432.7	1811.7	2.533
Coal Bed 5	2635.2	1384.9	1.711
Shale	3697.9	2000.6	2.547
Coal Bed 6	2982.5	1646.5	1.993

$$R_{PP}(\theta_1) \approx R_p + \left(A_0 R_P + \frac{\Delta\sigma}{(1-\sigma)^2} \right) \sin^2 \theta_1 + \frac{1}{2} \frac{\Delta V_P}{V_{Pa}} (\tan^2 \theta_1 - \sin^2 \theta_1), \quad (2.3)$$

and the Hilterman's approximation is

$$R_{PP}(\theta_1) \approx R_P \cos^2 \theta_1 + 2.25 \Delta\sigma \sin^2 \theta_1, \quad (2.4)$$

where,

R_{PP} = P-wave reflection coefficient,

$R_P = \frac{\rho_2 V_{P2} - \rho_1 V_{P1}}{\rho_2 V_{P2} + \rho_1 V_{P1}}$ = P-wave reflection coefficient at normal incidence

$p = \frac{\sin\theta_1}{V_{P1}} = \frac{\sin\theta_2}{V_{P2}} = \frac{\sin\phi_1}{V_{s1}} = \frac{\sin\phi_2}{V_{s2}}$ = ray parameter,

V_{P1} = P-wave velocity in medium 1,

V_{P2} = P-wave velocity in medium 2,

V_{S1} = S-wave velocity in medium 1,

V_{S2} = S-wave velocity in medium 2,

ρ_1 = density of medium 1,

ρ_2 = density of medium 2,

θ_1 = P-wave incident angle,

θ_2 = P-wave transmitted angle,

ϕ_1 = S-wave reflected angle,

ϕ_2 = S-wave transmitted angle,

$\sigma = \frac{\frac{1}{2}\left(\frac{V_P}{V_S}\right)^2 - 1}{\left(\frac{V_P}{V_S}\right)^2 - 1}$ = Poisson's ratio,

$\Delta\rho = \rho_2 - \rho_1$,

$\Delta\sigma = \sigma_2 - \sigma_1$,

$\Delta V_P = V_{P2} - V_{P1}$,

$\Delta V_s = V_{S2} - V_{S1}$,

$$\rho_a = (\rho_2 + \rho_1)/2,$$

$$V_{Pa} = (V_{P2} + V_{P1})/2,$$

$$V_{Sa} = (V_{S2} + V_{S1})/2,$$

$$\theta = (\theta_1 + \theta_2)/2,$$

$$A_0 = B_0 - 2(1 + B_0)\left(\frac{1-2\sigma}{1-\sigma}\right),$$

and

$$B_0 = \frac{\frac{\Delta V_p}{V_{Pa}}}{\frac{\Delta V_p}{V_{Pa}} + \frac{\Delta\rho}{\rho_a}}.$$

2.3.2 Full elastodynamic AVO modeling

Full elastodynamic AVO modeling (Virieux, 1986; Youn and Zhou, 1998) was performed to generate a synthetic CDP gather in order to evaluate composite amplitude responses of the whole lithologic column encountered at Well C. The P-wave velocity, S-wave velocity, and density logs from Well C were used without picking, editing, or blocking to simulate a total in-situ response at the well location. The actual surface seismic geometry of the 3D seismic survey acquired in 1998 was used for comparison with real data. The grid size of finite-difference elastodynamic AVO modeling was 1 m in depth and 5 m in offset. The 1-m grid in depth direction was intended to accommodate thin layers, especially the coal beds. The main parameters for the finite-difference full elastodynamic AVO modeling are shown in Table 2.4. Figure 2.2 shows a 40 Hz-Ricker wavelet that was used in the modeling (following the European polarity standard for a zero-phase wavelet).

The synthetic CDP gather was processed through spherical-divergence gain recovery, NMO corrections, and mute.

2.4 Phase correlation and phase rotation

Some differences in wavelet phase between real and synthetic data, although the surface seismic data has been zero-phased by a deterministic designature using a

Table 2.4 Main parameters used to stimulate the synthetic model.

Parameter	Value
Offset grid size	5 m
Depth grid size	1 m
Ricker wavelet period	0.025 s
Number of time sample	12500 (record length 2.5 sec)
Time sampling interval	0.0002 s
Number of receiver	40 receivers (40-fold CDP)
Number of source point	1 (point source)

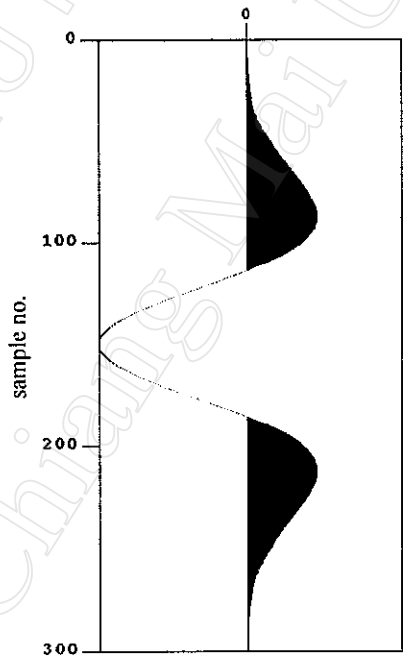

Figure 2.2 The 40 Hz-Ricker wavelet that was used in the elastodynamic modeling. Time zero is at 30 ms (sample number 150).

measured far-field signature, have been observed and analyzed. A phase and time-shift correlation program (developed at PTTEP) was used to evaluate cross-correlations between two traces for simultaneous changes in phase and time shift. After evaluating the best matching phase rotation angle and time shift amount, the real data were phase-rotated and time-shifted accordingly. I developed this phase rotation and time shifting software in C++ and Fortran languages. The programs listed in Appendix.

2.5 Elastic impedance

Elastic impedance (EI) is an approximation derived from a linearization of Zoeppritz equations, and is a function of P-wave velocity, S-wave velocity, density, and angle of incidence (Connolly, 1999). The *EI* equation is

$$EI(\theta) = V_p \left[V_S^{(\tan^2\theta)} V_S^{(-8K\sin^2\theta)} \rho^{(1-4K\sin^2\theta)} \right], \qquad (2.5)$$

where K is $\frac{V_S^2}{V_P^2}$.

EI(0) is equal to acoustic impedance (AI). To correlate with AVO angle stacks, EI(10) and EI(25) of gas sands, wet sands and coal beds were calculated.